

ChemComm

Accepted Manuscript



This article can be cited before page numbers have been issued, to do this please use: G. Tang, S. Wang, W. Lv, M. Liu, H. Zeng, Z. Chen, J. Dong, Z. Wu, X. Feng and W. Zeng, *Chem. Commun.*, 2018, DOI: 10.1039/C7CC09806E.



This is an Accepted Manuscript, which has been through the Royal Society of Chemistry peer review process and has been accepted for publication.

Accepted Manuscripts are published online shortly after acceptance, before technical editing, formatting and proof reading. Using this free service, authors can make their results available to the community, in citable form, before we publish the edited article. We will replace this Accepted Manuscript with the edited and formatted Advance Article as soon as it is available.

You can find more information about Accepted Manuscripts in the [author guidelines](#).

Please note that technical editing may introduce minor changes to the text and/or graphics, which may alter content. The journal's standard [Terms & Conditions](#) and the ethical guidelines, outlined in our [author and reviewer resource centre](#), still apply. In no event shall the Royal Society of Chemistry be held responsible for any errors or omissions in this Accepted Manuscript or any consequences arising from the use of any information it contains.



Journal Name

COMMUNICATION

A self-assembled nanoprobe for the long term cancer cell nucleus-specific staining and two-photon breast cancer imaging

Received 00th January 20xx,
Accepted 00th January 20xx

DOI: 10.1039/x0xx00000x

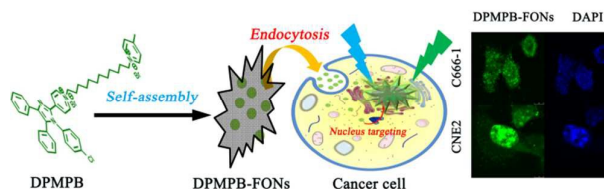
www.rsc.org/

Tang Gao^{a,1}, Shuanglian Wang^{b,1}, Wuwu Lv^b, Mian Liu^b, Hongliang Zeng^a, Zhu Chen^a, Jie Dong^a, Ziping Wu^a, Xueping Feng^{b,*}, Wenbin Zeng^{a,*}

Herein, a novel self-assembled nanoprobe for long-term tracking nucleolus of cancer cells and differentiating clinical breast cancer tissues and para-carcinoma tissues has been developed.

As the most prominent organelle within cells, nucleolus regulates ribosome synthesis and gene expression.^[1] It reported that the nuclei of cancer cells have distinguished architecture compared with the nuclei of normal cells.^[2] Therefore, fluorescence nucleus imaging in live cells is not only to gain insights into the process of malignant transformation of tumour, but also to provide a basis for developing new diagnostic and therapeutic tools for cancer.^[3] The well-known organic dyes, including 4',6-diamidino-2-phenylindole (DAPI), propidium iodide (PI) and Hoechst, have been widely used to stain nuclei of cancer or normal cells. However, these fluorophores are generally mutagenic with potential health hazards and often suffer from low water solubility, poor photostability, which limit their further application such as long-term imaging of nuclei.^[4] Furthermore, though quantum dots have been widely used to image nuclei, they have intrinsic toxicity^[5] and cannot penetrate into nucleus without surface modification.^[6] Small organic fluorophores, used for the cell nucleolus imaging, such as styryl dyes,^[7] fluorescein,^[9] ruthenium (II)^[10] and hemicyanine derivatives,^[11] are often used at very low concentration because of the limitation of aggregation-caused quenching (ACQ) effect. Unfortunately, these dyes are found to be easily photo-bleach upon photoexcitation,^[12] which also inhibit their applications in long-term monitoring the cell nucleus.^[13] Therefore, it is highly desirable to design novel fluorescent probes with high water solubility, good photostability, low cytotoxicity and overcome the effect of ACQ to achieve long-term cellular nucleus imaging. Recently, based on tetraphenyl imidazole-cored molecular

rotors, our group developed a novel series of AIEgens with good photo-stability, high water solubility, and good biocompatibility.^[14] Based on the previous work, we intend to develop novel fluorescent probes that can long term selectively stain the nuclei of cancer cells. The physicochemical properties of probes that facilitate nucleic acid binding include cationic characteristics and planar aromatic systems. Probes that allow access to cells are characterized by low protein and lipid binding. Reduced non-nuclear site build up characteristics include cationic high alkalinity and hydrophilicity.^[15] The quaternary ammonium salt, an electron accepting group with positively charged, can promote the probe into the cell due to lipophilicity and electrophoretic forces.^[16] Furthermore, AIEgens with superior photostability and excellent biological application may aggregate in cell nucleus and emit strong fluorescence,^[17] which could be utilized for long-term tracing cancer cells with low-toxicity.^[18] Take above into consideration, in this paper we designed and synthesized a novel water soluble cationic bola-type small molecule 4-(1-(4-chlorophenyl)-4,5-diphenyl-1H-imidazol-2-yl)-1-(12-(pyridin-1-ium-1-yl)dodecyl)pyridin-1-ium bromide denoted as DPMPB which can be self-assembled into positively charged nanoparticles (DPMPB-FONs) with weak emission in aqueous solution, and selectively stain the nuclei of cancer cells in a long time (Figure 1). Remarkably, the applicability of DPMPB to image breast cancer and para-carcinoma tissue highlighted the potential as a guiding-agent in surgery.



Scheme 1. Schematic illustration of DPMPB as a fluorescent nanoprobe for selective nucleus imaging in cancer cells.

The synthetic route to DPMPB was shown in Scheme S1. 2-Hydroxy-1, 2-diphenylethanone (compound 1) was prepared by thiamine hydrochloride-mediated benzoin condensation

^a Xiangya School of Pharmaceutical Sciences, Central South University, Changsha 410013, China. wbzeng@hotmail.com.

^b Institute of Medical Sciences, Xiangya Hospital, Central South University, Changsha 410078, China. fxp1029@aliyun.com.

¹ These authors contributed equally.

Electronic Supplementary Information (ESI) available: [details of any supplementary information available should be included here]. See DOI: 10.1039/x0xx00000x

reaction. Oxidation of compound **1** afforded the corresponding benzil. 4-(1-(4-Chlorophenyl)-4, 5-diphenyl-1H-imidazol-2-yl) pyridine (compound **3**) was achieved by a one-pot two-steps multicomponent reaction of 4-pyridinecarboxaldehyde, p-chloroaniline, benzyl and ammonium acetate. Compound **3** was reacted with 1-(12-bromododecyl)-4-methylpyridin-1-ium bromide (compound **4**) to yield **DPMPB**. The detailed syntheses and characterization of **DPMPB** and the intermediates are given in the supporting information.

With **DPMPB** in hand, we firstly investigated its optical properties. Due to the hydrophilic nature of the Py salt, **DPMPB** has good solubility in polar solvents such as dimethyl sulfoxide, acetonitrile, methanol and water. As shown in **Figure S1**, **DPMPB** exhibits an absorption band at around 400 nm, irrespective of the type of solvent used. The absorption band at around 400 nm may attribute to the intramolecular charge transfer (ICT) transition between the electron donating imidazole and the electron-withdrawing Py salt. The fluorescence emission spectra of **DPMPB** shown obvious polarity dependence upon in different solvents upon excited with 385 nm (**Figure S2a**). It showed strong emission at around 495 nm with larger Stokes shift (110 nm) in lower polarity index media solution such as dioxane and tetrahydrofuran. By contrast, the emission of **DPMPB** weakened and red shifted in higher polarity index media (DMSO, CH₃CN, CH₃OH and H₂O). As anticipated, the solvent effect was derived from the ICT effect. In order to further investigate the ICT interaction between the pyridinium substituent and imidazole, the computational calculations were performed. As shown in **Figure S2b**, the electron-donating imidazole unit has a higher electron in the highest occupied molecular orbital (HOMO). While, in the lowest unoccupied molecular orbital (LUMO) the electron density tends to be denser around the pyridinium segment. It is clear that there is strong electron interaction to allow the flow of electrons from imidazole unit to pyridinium segment, resulting in a large ICT effect in **DPMPB**. After that, we investigated the AIE properties of **DPMPB**. As shown in **Figure 1a**, in dilute water solution, **DPMPB** showed a faint green fluorescence. In contrast, upon increasing the THF fraction to 90 Vol%, the emission of **DPMPB** increased. Furthermore, when the fraction of THF up to 100% a strong emission peak at 495 nm was detected and bright green fluorescence was observed under 365 nm UV illumination from a hand-held UV lamp (**Figure 1b** inset). The high THF fraction induces a dramatic increase in fluorescence, which confirms the AIE property of **DPMPB**. In order to prove the high emission in high THF portion solution was attributed to AIE effect. By increasing the concentration of **DPMPB** from 5 μ M to 90 μ M, the fluorescence intensity increased, suggesting that **DPMPB** started to form aggregates (**Figure S3**). Such emission is possibly attributed to the aggregation of **DPMPB** and activates the RIR process. The quantum yield (QY) of **DPMPB** in pure THF was 14.2%. Compared to the quenched in the solid state of traditional fluorescent dyes, **DPMPB** solid powder emits the stronger green light under the excitation of ultraviolet light (**Figure 1a** inset). The excellent optical property makes **DPMPB** suitable for fluorescence imaging

studies. To explore the aggregation of **DPMPB** in aqueous, we performed the experiments of dynamic light scattering (DLS) and scanning electron microscopy (SEM). The DLS studies indicated the aggregates of **DPMPB** have an average diameter of 219 nm with PDI 0.160 (**Figure 1c**). As shown in **Figure 1d**, the compound **DPMPB** could self-assemble into spherical nanoaggregates (**DPMPB-FONs**). The aggregates states with faint emission may be ascribed to the formation of loosely packed with enough free volume to consume the radiative energy by the intramolecular rotation.^[19] Furthermore, the zeta potential experiments indicated that **DPMPB-FONs** had an average zeta potential of 3.70 mV in PBS (**Figure S4**), which may be attributed to the presence of cationic pyridinium. This positive charge may improve the ability of **DPMPB-FONs** to enter tumour cells through charge-mediated endocytosis.^[20]

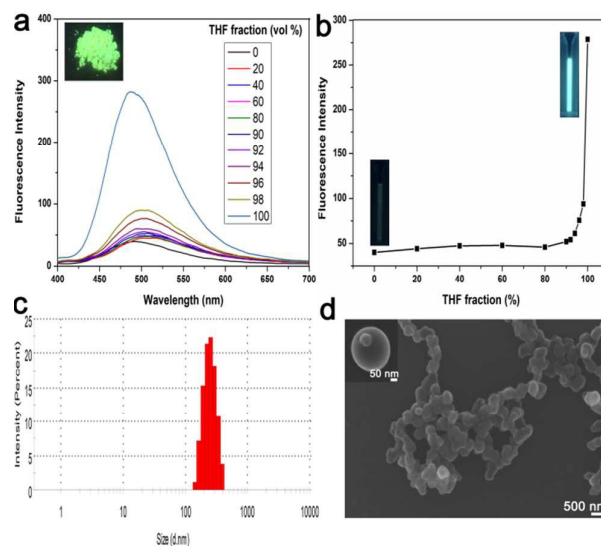


Figure 1. (a) Fluorescent emission spectra of **DPMPB** (5 μ M) in THF-water mixtures with different THF fractions (fw). inset: Photograph of **DPMPB** solid powder taken under portable UV lamp 365 nm illumination. (b) Plots of fluorescent intensity vs. THF fractions of **DPMPB**, (c) DLS size distribution of **DPMPB-FONs** (5 μ M) in an aqueous solution. (d) SEM image of **DPMPB-FONs**.

It is reported that the difference in mitochondrial membrane potential between normal epithelial cells and carcinoma cells is at least 60 mV. In addition to mitochondrial membrane potential, plasma membrane potential is also higher in carcinoma cells than in normal epithelial cells.^[21] Thus, due to the stronger electrostatic interaction and charge-mediated endocytosis, we hypothesized that **DPMPB-FONs** will be more internalized and accumulated in cancer cells than normal cells. To verify this hypothesis, nasopharyngeal carcinoma cells C666-1, CNE2, adenocarcinoma gastric cells AGS and normal gastric mucosa cells GES-1 were incubated with **DPMPB-FONs** under the same conditions. As shown in **Figure S5**, strong greenish fluorescence was observed in cancerous cells (C666-1, CNE2 and AGS) after incubation of 30 min. In sharp contrast, the faint fluorescence was observed in

GES-1 cells (Figure S5d). In addition, after incubation of 22 and 29 hours cancer cells (C666-1, CNE2 and AGS) still exhibited strong fluorescence (Figure S6), and the results showed that the DPMPB-FONs could be used for long-term fluorescence imaging of cancer cells. The location and distribution of DPMPB-FONs in living cells was further explored by confocal scanning laser microscopy. Four kinds of cells, including three cancer cells (C666-1, CNE2 and AGS) and one normal cell (GES-1), were employed as a cell model and were co-stained with DPMPB-FONs and DAPI for 4 h. As shown in Figure 2, in all three kinds of cancer cells, the green fluorescence from DPMPB-FONs overlaps well with the blue fluorescence of DAPI. In contrast, no greenish emission of DPMPB-FONs was observed in living cells of GES-1 (Figure S7). These results indicated that DPMPB-FONs not only can distinguish between cancer cells and normal cells, but also specifically target the nucleolus of cancer cells. Nucleuses, the most prominent cellular organelle, are closely associated with diseased phenotypes,^[22] and many of anticancer drugs are target to the nucleus. Thus, fluorescent probes targeted to nucleus for a long period time are very helpful to acquire crucial diagnostic and prognostic information.^[23] In our study, the long-term tracking nucleolus ability of DPMPB-FONs was also determined. As seen from Figure S8, we can see that the green fluorescence was collected from the nucleus region and overlap well with the blue fluorescence of DAPI until incubation of 112 hrs. Furthermore, in such a long incubation time, the shape of the nucleus did not change significantly. These results further confirmed that DPMPB-FONs show low cytotoxicity and can be effectively internalized into cancer cells and have the ability to track cancer nucleoli for a long time. To investigate the light-up response of DPMPB-FONs in cell nucleus, fluorescence spectra were explored when DNA was added into the DPMPB-FONs in PBS buffer solution (pH = 7.4). As seen from Figure S9a, the fluorescence intensity of DPMPB-FONs rises significantly with increasing amount of DNA and reaches a maximum at 8 $\mu\text{g}/\text{mL}$. The observed fluorescence enhancement may owe to the electrostatic interactions between the oppositely charged DPMPB-FONs and DNA, resulting in blocking the free rotation of DPMPB molecules.^[24] Moreover, the fluorescence intensity at 500 nm and DNA concentrations exhibited a good linearity relationship ($R^2 = 0.981$) in the range of 0 to 8 $\mu\text{g}/\text{mL}$ (Figure S9b). This result demonstrated that the DPMPB-FONs can sensitively detect DNA in water solution. The cytotoxicity of DPMPB-FONs on GES-1 cells was also evaluated by CCK-8 assay. As shown in Figure S10, the cell viability was tested after the incubation with various concentrations of DPMPB-FONs (0–20 μM) for 48 h. The cell viability remains above 62% high at DPMPB-FONs concentrations as high as 20 μM , indicating low cytotoxicity of DPMPB-FONs in the test and suitable for the application in the long-term tracing.

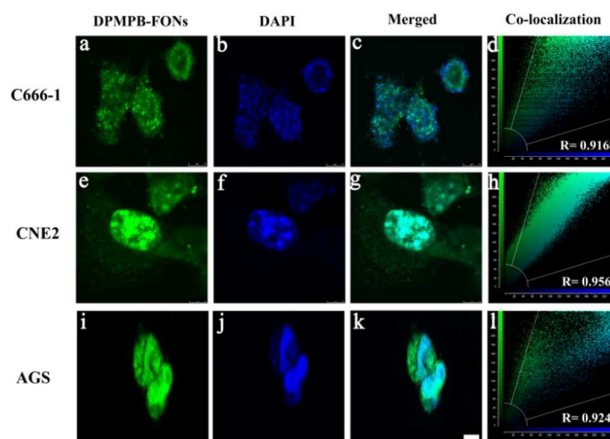


Figure 2. Confocal laser fluorescence microscopic images of C666-1, CNE2 and AGS cells treated with 5 μM DPMPB-FONs and DAPI (1.0 μM), respectively. a), e) and i) Fluorescence imaging of DPMPB-FONs in C666-1, CNE2 and AGS cells, respectively collected at 480–530 nm and excited at 400 nm. b), f) and j) Fluorescence image of DAPI in C666-1, CNE2 and AGS cells, respectively collected by a 450–470 nm band path filter with excitation at 358 nm. c), g) and k) Merged image of C666-1, CNE2 and AGS cells, respectively. d), h) and l) Correlation plot of DAPI and DPMPB-FONs intensities. Scale bar: 7.5 μm .

Surgical operation is the primary treatment modality for most solid tumours. Traditionally, tumour removal during surgery relies on the experience of the surgeons to differentiate tumour from normal tissue, which is not easily quantifiable and do not offer the sensitivity to identify the tumour margins.^[25] Hence, the way to objectively assess tumour margins during surgery would be of great value. Optical image-guided surgery was proven to be significant potential to objectively assess the tumour margin and guide the surgeon to adequately resect the tumour.^[26] The success of illuminating cancer cells inspired us to further use our probe in cancer tissue and normal tissue. The breast cancer tissue and para-carcinoma tissue were removed from a 44-year-old patient with breast cancer. As shown in Figure S11, the fluorescence of para-carcinoma tissue is obviously weaker than the cancer tissues when observed by using fluorescence microscope. The results indicated that DPMPB-FONs were capable of specific staining of the cancer tissue with high contrast. It is noted that, the short excitation wavelengths have shallow tissue penetration depths and their application is limited. In comparison with one-photon imaging, two-photon imaging can provide better three-dimensional spatial localization, higher imaging resolution, and increased penetration depth.^[27] We then further investigated the utility of DPMPB-FONs in deep breast cancer tissue and para-carcinoma tissue. The fluorescence images were obtained by two-photon confocal microscopy, and the images of breast cancer and para-carcinoma tissues stained with DPMPB-FONs were recorded at green emission channels. The breast cancer and para-carcinoma tissues stained with DAPI were collected at blue emission channels. As shown in Figure 3a, 3D

reconstruction fluorescence images of breast cancer tissue stained with **DPMPB-FONs** exhibited strong green fluorescence, which has a good overlap with the blue fluorescence stained with **DAPI** (Figure 3c). In contrary, paracarcinoma tissues stained with **DPMPB-FONs** showed faint green fluorescence, which is almost no overlap with the blue fluorescence stained with **DAPI** (Figure S12). These results further demonstrated that **DPMPB-FONs** have an excellent selectivity for tumour tissue. In addition, the confocal Z-scan two-photon imaging sections at different penetration depths exhibited bright two-photon excited Fluorescence signal down to 100 μm of the penetration depth (Figure 3e), indicating that **DPMPB-FONs** has the deep tissue imaging capability.

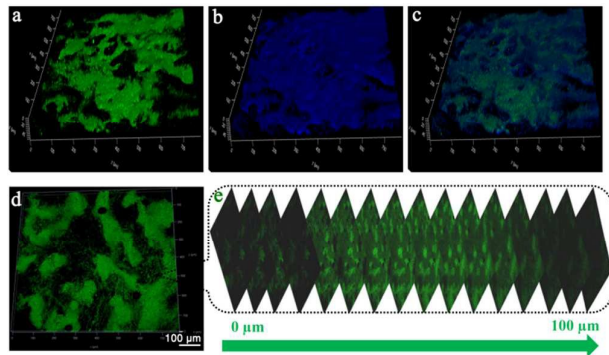


Figure 3. (a) 3D reconstruction fluorescence images of breast cancer tissue stained with 5 μM of **DPMPB-FONs** in two-photon mode by collecting the emissions at 480–530 nm upon excitation at 760 nm. (b) 3D projection fluorescence images of breast cancer tissue stained with 1 μM **DAPI** by collecting the emissions at 450–470 nm upon excitation at 358 nm. (c) Merged image of (a) and (b). (d) 3D reconstruction from 50 confocal Z-scan two-photon excited imaging sections at depth of 0–100 μm (e) Sectional TPM images of breast cancer tissue labelled with **DPMPB-FONs** (5 μM) from the mucosal surface (0 μm) to 100 μm depth. Scale bar: 100 μm .

In conclusion, we have developed a novel bola type of molecule **DPMPB** with AIE characteristics, high water solubility and excellent optical properties. **DPMPB** can self-assemble into positively charged spherical structure of nanoparticles (**DPMPB-FONs**) with weak emission in aqueous solution. Due to the strong electrostatic interaction and charge-mediated endocytosis, **DPMPB-FONs** can selectively stain the cancer cells but not normal ones. The colocalization experiments proved that **DPMPB-FONs** could specifically target the nucleolus of cancer cells. Furthermore, owing to the excellent spectral properties, **DPMPB-FONs** have the ability of long-term tracking nucleolus of cancer cells. The cytotoxicity tests demonstrated that **DPMPB-FONs** have low cytotoxicity. Additionally, **DPMPB-FONs** are capable of differentiating clinic breast cancer tissues from para-carcinoma tissues with high fluorescence contrast. More importantly, **DPMPB-FONs** can be successfully used to two-photon imaging breast cancer tissues at a depth of approximately 100 μm . Due to the fact that **DPMPB-FONs** can selectively distinguish cancer cells from normal cells, **DPMPB-FONs** have the potential of as a guiding-agent in surgery.

Acknowledgements

We are grateful for the financial supports from National Natural Science Foundation of China (81741134, 81671756 and 81372905), Hunan Provincial Natural Science Foundation of China (2015JJ4075), and Key Research Project of Science and Technology Foundation of Hunan Province (2017SK2093).

Notes and references

- M. M. Yusupov, G. Z. Yusupova, A. Baucom, K. Lieberman, T. N. Earnest, J. Cate, H. F. Noller, *Science*, 2001, **292**, 883.
- R. W. Ruddon, *Cancer Biology*, Oxford University Press, 2007.
- D. Zink, A. H. Fischer, J. A. Nickerson, *Nat. Rev. Cancer*, 2004, **4**, 677.
- R. M. Martin, H. Leonhardt, M. C. Cardoso, *Cytom. Part. A*, 2005, **67**, 45.
- A. M. Delfus, W. C. Chan, S. N. Bhatia, *Nano. Lett.*, 2004, **4**, 11.
- D. Zhao, Z. He, P. S. Chan, R. N. Wong, N. K. Mak, A. W. Lee, W. H. Chan, *J. Phys. Chem. C*, 2010, **114**, 6216.
- Q. Li, Y. Kim, J. Namm, A. Kulkarni, G. R. Rosania, Y.-H. Ahn, Y.-T. Chang, *Chem. Biol.*, 2006, **13**, 615.
- G. Song, Y. Sun, Y. Liu, X. Wang, M. Chen, F. Miao, W. Zhang, X. Yu, J. Jin, *Biomaterials*, 2014, **35**, 2103.
- N. Stevens, N. O'connor, H. Vishwasrao, D. Samaroo, E. R. Kandel, D. L. Akins, C. M. Drain, N. J. Turro, *J. Am. Chem. Soc.*, 2008, **130**, 7182.
- N. A. O'Connor, N. Stevens, D. Samaroo, M. R. Solomon, A. A. Martí, J. Dyer, H. Vishwasrao, D. L. Akins, E. R. Kandel, N. J. Turro, *Chem. Commun.*, 2009, **19**, 2640.
- J. T. Miao, C. Fan, R. Sun, Y. J. Xu, J. F. Ge, *J. Mater. Chem. B*, 2014, **2**, 7065.
- X. Ma, R. Sun, J. Cheng, J. Liu, F. Gou, H. Xiang, X. Zhou, *J. Chem. Edu.*, 2015, **93**, 345.
- A. Chaumet, G. D. Wright, S. H. Seet, K. M. Tham, N. V. Gounko, F. Bard, *Nat. Commun.*, 2015, **6**, 8218.
- (a) T. Gao, X. Cao, P. Ge, J. Dong, S. Yang, H. Xu, Y. Wu, F. Gao, W. Zeng, *Org. Biomol. Chem.*, 2017, **15**, 4375. (b) T. Gao, X. Cao, J. Dong, Y. Liu, W. Lv, C. Li, X. Feng, W. Zeng, *Dyes Pigments*, 2017, **143**, 436; (c) T. Gao, S. Yang, X. Cao, J. Dong, N. Zhao, P. Ge, W. Zeng, Z. Cheng, *Anal. Chem.*, 2017, **89**, 10085.
- R. W. Horobin, J. C. Stockert, F. Rashid-Doubell, *Histochem. Cell Biol.*, 2006, **126**, 165.
- H. Ma, Z. Yang, H. Cao, L. Lei, L. Chang, Y. Ma, M. Yang, X. Yao, S. Sun, Z. Lei, *J. Mater. Chem. B*, 2017, **5**, 655.
- J. Mei, N. L. Leung, R. T. Kwok, J. W. Lam, B. Z. Tang, *Chem. Rev.*, 2015, **115**, 11718.
- Z. Wang, S. Chen, J. W. Lam, W. Qin, R. T. Kwok, N. Xie, Q. Hu, B. Z. Tang, *J. Am. Chem. Soc.*, 2013, **135**, 8238.
- A. Shao, Z. Guo, S. Zhu, S. Zhu, P. Shi, H. Tian, W. Zhu, *Chem. Sci.*, 2014, **5**, 1383.
- H. Wang, Y. Li, H. Bai, J. Shen, X. Chen, Y. Ping, G. Tang, *Adv. Funct. Mater.*, 2017, **27**, 1700339.
- L. B. Chen, *Ann. Rev. Cell Biol.*, 1988, **4**, 155.
- A. I. Lamond, W. C. Earnshaw, *Science*, 1998, **280**, 547.
- M. R. Gill, J. Garcia-Lara, S. J. Foster, C. Smythe, G. Battaglia, J. A. Thomas, *Nat. Chem.*, 2009, **1**, 662.
- J. Liang, G. Feng, R. T. K. Kwok, D. Ding, B. Tang, B. Liu, *Sci. China Chem.*, 2016, **59**, 53.
- A. L. Vahrmeijer, M. Hutteman, J. R. Van Der Vorst, C. J. Van De Velde, J. V. Frangioni, *Nat. Rev. Clin. Oncol.*, 2013, **10**, 507.
- Q. T. Nguyen, E. S. Olson, T. A. Aguilera, T. Jiang, M. Scadeng, L. G. Ellies, R. Y. Tsien, *Procd. Natl. Acad. Sci. USA*, 2010, **107**, 4317.
- (a) H. M. Kim, B. R. Cho, *Chem. Rev.*, 2015, **115**, 5014; (b) H.-W. Liu, S. Xu, P. Wang, X.-X. Hu, J. Zhang, L. Yuan, X.-B. Zhang and W. Tan, *Chem. Commun.*, 2016, **52**, 12330.